



Published in final edited form as:

*Neuroimage*. 2009 August 15; 47(2): 602–610. doi:10.1016/j.neuroimage.2009.04.053.

## Linking Functional and Structural Brain Images with Multivariate Network Analyses: A Novel Application of the Partial Least Square Method

Kewei Chen, Ph.D.<sup>1,2,9</sup>, Eric M. Reiman, M.D.<sup>1,4,5,9</sup>, Zhongdan Huan, Ph.D.<sup>6</sup>, Richard J. Caselli, M.D.<sup>8,9</sup>, Daniel Bandy, MS<sup>1,9</sup>, Napatkamon Ayutyanont, Ph.D.<sup>1,9</sup>, and Gene E. Alexander, Ph.D.<sup>7,9</sup>

<sup>1</sup> Banner Alzheimer's Institute and the Banner Good Samaritan PET Center, Phoenix, AZ, USA

<sup>2</sup> The Dept of Math and Statistics, Arizona State Univ

<sup>4</sup> The Dept of Psychiatry, University of Arizona, Tucson

<sup>5</sup> The Translational Genomics Research Institute, Phoenix, USA

<sup>6</sup> School of Mathematical Sciences, Beijing Normal Univ, Beijing, China

<sup>7</sup> The Dept of Psychology and Evelyn F. McKnight Brain Institute, Univ of Arizona, Tucson

<sup>8</sup> The Mayo Clinic, Scottsdale

<sup>9</sup> The Arizona Alzheimer's Consortium, Phoenix, Arizona, USA

### Abstract

In this article, we introduce a multimodal multivariate network analysis to characterize the linkage between the patterns of information from the same individual's complementary brain images, and illustrate its potential by showing its ability to distinguish older from younger adults with greater power than several previously established methods. Our proposed method uses measurements from every brain voxel in each person's complementary co-registered images and uses the partial least square (PLS) algorithm to form a combined latent variable that maximizes the covariance among all of the combined variables. It represents a new way to calculate the singular value decomposition from the high-dimensional covariance matrix in a computationally feasible way. Analyzing fluorodeoxyglucose positron emission tomography (PET) and volumetric magnetic resonance imaging (MRI) images, this method distinguished 14 older adults from 15 younger adults ( $p = 4e-12$ ) with no overlap between groups, no need to correct for multiple comparisons, and greater power than the univariate Statistical Parametric Mapping (SPM), multimodal SPM or multivariate PLS analysis of either imaging modality alone. This technique has the potential to link patterns of information among any number of complementary images from an individual, to use other kinds of complementary complex datasets besides brain images, and to characterize individual state- or trait-dependent brain patterns in a more powerful way.

---

Corresponding author: Kewei Chen, Ph.D., Banner Good Samaritan PET Center, 1111 E. McDowell Road, Phoenix, Arizona 85006, USA; telephone: 602-239-4851; fax: 602-239-3073; e-mail: E-mail: kchen@math.la.asu.edu, and E-mail: Kewei.chen@bannerhealth.com.

**Publisher's Disclaimer:** This is a PDF file of an unedited manuscript that has been accepted for publication. As a service to our customers we are providing this early version of the manuscript. The manuscript will undergo copyediting, typesetting, and review of the resulting proof before it is published in its final citable form. Please note that during the production process errors may be discovered which could affect the content, and all legal disclaimers that apply to the journal pertain.

## INTRODUCTION

Although clinical and research studies commonly acquire complementary brain images from each participant, the statistical analyses in most studies are performed with the data from different images analyzed separately (i.e., “unimodal” analyses), and often use “univariate” methods that treat different voxels or regions-of-interest (ROIs) within an image as independent. Advances in image-analysis techniques have made it possible to use one image modality to help support the analysis of a complementary image modality. For instance, co-registered magnetic resonance images (MRI) can be used to localize anatomical ROIs in functional brain images, support the anatomical deformation and standardization of functional brain images, characterize functional brain imaging measurements in segmented brain tissues and help correct them for the effects of partial-volume averaging, and characterize the correlations between regional measurements in the complementary datasets (Ashburner and Friston, 1997; Casanova et al., 2007; Ibanez et al., 1998; Jack, Jr. et al., 2008). Despite these and other advances, analytical methods are needed to more fully capitalize on the patterns of information from potentially complementary, complex data sets acquired from the same individual.

In contrast to univariate image-analysis methods, multivariate image-analysis techniques can be used to characterize voxel- or region-based patterns of covariance. For instance, multivariate image-analysis methods have been used to analyze patterns (or networks) of the regional cerebral metabolic rate for glucose (CMRgl) in fluorodeoxyglucose positron emission tomography (FDG PET) and gray matter volume in magnetic resonance images (MRI), as well as patterns of activation in  $^{15}\text{O}$ -water PET images and functional MRI (fMRI) (Alexander et al., 1999; Alexander and Moeller, 1994; Feigin et al., 2001; Habeck et al., 2005; McKeown and Sejnowski, 1998; Moeller et al., 1987; Smith et al., 2006; Alexander et al., 2006; McIntosh et al., 1996; Alexander et al., 2008). Multivariate image-analysis methods include principal component analysis (PCA) (Friston, 1994), the PCA-based Scaled Subprofile Model (SSM), independent component analysis (Calhoun et al., 2001; Calhoun et al., 2003; Chen et al., 2002; Esposito et al., 2003; McKeown and Sejnowski, 1998; Moritz et al., 2000; Schmithorst and Holland, 2004), the Partial Least Squares (PLS) method (McIntosh et al., 1996; Worsley et al., 1997), structural equation modeling (McIntosh and Gonzalez-Lima, 1994), ordinal trend analysis (Habeck et al., 2005), and dynamic causal modeling (Friston et al., 2003). These methods have typically been used to characterize regional networks of brain function or structure and to test their ability to distinguish between groups, states, and/or their interactions, or to relate patterns of measurements or activation to other (e.g., cognitive, behavioral, or biological) measurements. These methods have been mostly used in ‘unimodal’ data analyses.

Efforts to apply multivariate image-analysis techniques to simultaneously characterize multimodal neuroimaging data have been applied successfully to time series of electroencephalography (EEG) and functional MRI (fMRI) (Martinez-Montes et al., 2004). Using multi-way PLS approach, the authors attempted to decompose simultaneously the EEG data into sum of spatial, temporal and spectral components and the fMRI into sum of spatial and temporal ones. The decomposition was constrained to maximize the covariance of corresponding temporal components between EEG and fMRI. The authors of that study concluded that fusing fMRI and EEG meaningfully extends the spatio-temporal resolution and sensitivity of each of these complementary datasets.

In this article, we introduce a multimodal multivariate data analysis technique to simultaneously characterize the linkage between the patterns of information from the same individual’s complementary brain images. We illustrate its potential value by showing its superiority to conventional methods in distinguish between older and younger adults using FDG PET and structural MRI, while resulting in similar age-related patterns within each of

the two imaging modalities. In addition to its recent multimodal application discussed above (Martinez-Montes et al., 2004), PLS was originally introduced to characterize the pattern of regional covariance within a single image modality (McIntosh et al., 1996), and has been used to identify regional patterns of functional brain imaging measurements that best distinguish different subject groups, states or traits (Anderson et al., 2000; Grady et al., 1998; Habib et al., 2003; Iidaka et al., 2000; Keightley et al., 2003; McIntosh, 1998; McIntosh, 1999; Nestor et al., 2002; O'Donnell et al., 1999; Rajah et al., 1999).

Here, we use PLS to simultaneously characterize the linkage between the same individuals' patterns of resting CMRgl using FDG PET and gray matter using volumetric MRI pattern of gray matter, applying the method in both an “agnostic” way, blind to known information of variable of interest (such as the subjects' characteristics or group membership) and in an “informed” way, which incorporates the known information of variable of interest about the subjects. Finally, to illustrate the potential of this multimodal multivariate image analysis technique, we compare it to conventional unimodal univariate and multivariate analyses in the discrimination between older and younger age groups.

We take the advantage of the fact that number of subjects is always much smaller than the number of voxels in the neuroimaging studies (so the rank of the covariance matrix is much lower than its size) to address the computational efficiency of the agnostic multimodal PLS method. We then focus our attention on implementing statistical procedures to assess type-I error for multimodal PLS based imaging markers. In addition, we illustrate how the multimodal PLS can be used to classify subjects in relationship to categorical older and young group memberships. Finally, we compare our new method to the independent unimodal analysis of PET or MRI using unimodal SPM, voxel-wise multimodal SPM, and unimodal, informed PLS analyses.

## MATERIALS AND METHODS

### Subjects and data

FDG PET and volumetric MRI images from 15 younger adults, 20–39 ( $31 \pm 5$ ) years of age, and 14 cognitively normal older adults, 65–80 ( $71 \pm 4$ ) years of age are used to evaluate the ability of the multimodal PLS to discriminate between these two age groups and compare it to some widely used unimodal univariate and multivariate methods. To minimize the potentially confounding contribution of preclinical brain changes, the study is restricted to non-carriers of the apolipoprotein E (APOE)  $\epsilon^4$  allele, a common Alzheimer's disease (AD) susceptibility gene (Reiman et al., 2004). The subjects agreed that they would not be given information about their APOE genotype, provided their informed consent, and were studied under guidelines approved by the institutional review boards at Banner Good Samaritan Medical Center (Phoenix, AZ) and the Mayo Clinic (Rochester, MN). PET images from the younger subjects were described in a previous comparison between younger and older carriers and non-carriers of the APOE  $\epsilon^4$  allele (Reiman et al., 2004).

The subjects denied memory concerns, did not satisfy criteria for a current psychiatric disorder, and did not use centrally acting medications for at least six weeks before their imaging sessions. Investigators who were unaware of the subjects' APOE genotype obtained data from medical and family histories, a neurological examination, and a structured psychiatric interview. All of the subjects completed the Folstein-modified Mini-Mental State Examination (MMSE) and the Hamilton Depression Rating Scale and all but one subject completed a battery of neuropsychological tests. All had a normal neurological examination. There were no significant differences between the younger and older age groups in their gender distribution (3 males and 12 females versus 5 males and 9 females, respectively,  $P=0.34$ ), but the older group had a slightly lower educational level ( $16.2 \pm 1.2$  and  $14.7 \pm 1.9$  years, respectively,  $P=0.019$ ). In this

methodology oriented study, no attempt was made separate the education effects in contrasting the two age groups.

PET was performed with the 951/31 ECAT scanner (Siemens, Knoxville, Tenn.), a 20-minute transmission scan, the intravenous injection of 10 mCi of  $^{18}\text{F}$ -FDG, and a 60-min dynamic sequence of emission scans as the subjects, who had fasted for at least 4 hours, lay quietly in a darkened room with their eyes closed and directed forward. PET images were reconstructed using the back projection with Hanning filter of 0.40 cycles per pixel and measured attenuation correction, resulting in 31 slices with in-plane resolution of about 8.5mm, full width at half maximum (FWHM), an axial resolution of 5.0–7.1mm FWHM, a 3.375 slice thickness and a 10.4cm axial field of view.

MRI was performed using a 1.5 T Signa system (General Electric, Milwaukee, WI) and a T1-weighted, three-dimensional pulse sequence (radio-frequency-spoiled gradient recall acquisition in the steady state [SPGR], repetition time =33 msec, echo time = 5 msec,  $\alpha=30^\circ$ , number of excitations=1, field of view=24cm, imaging matrix=256 by 192, slice thickness=1.5mm, scan time=13:36 min). The MRI data set consisted of 124 contiguous horizontal slices with in-plane voxel dimension of 0.94 by 1.25mm.

### Data pre-processing

SPM2 (<http://www.fil.ion.ucl.ac.uk/spm/>) was used for image pre-processing. Automated segmentation and normalization procedures (Good et al., 2001) were applied to each subject's MRI to exclude non-brain tissue and to generate maps of smoothed gray matter density after spatial deformation into Montreal Neurological Institute (MNI) template space. A common mask was created and applied to the segmented gray matter density maps to include gray matter voxels with an intensity value of at least 0.2 in every subject for subsequent analyses. Automated algorithms were also applied to each subject's PET image, co-registering it to the subject's MRI and deforming it into MNI template space using the normalization parameters derived using the MRI segmentation and normalization procedures noted above. The PET images were then resampled to the same slice, matrix, and voxel size and number, and filtered using the same mask. Finally, PET and MRI images were each smoothed to 15 mm FWHM.

To create  $X_{\text{MRI}}$  and  $X_{\text{PET}}$  numerical matrices for subsequent PLS analysis, each respective MRI or PET voxel within the brain mask was labeled as voxel 1, voxel 2, ..., voxel  $P_X$  (where  $P_X$  is the number of voxels inside the brain mask). At each given voxel location, a column vector of length  $n$ , where  $n$  is the number of subjects ( $n=29$  for our current study), was formed whose element  $i$  is the voxel intensity from subject  $i$  ( $i=1, \dots, n$ ). The agnostic multimodal PLS was used to identify the linkage between  $X_{\text{PET}}$  (which we treated as the dependent data block) and  $X_{\text{MRI}}$  (which we treated as independent data block). The informed multimodal PLS uses the combined matrix  $[X_{\text{PET}} X_{\text{MRI}}]$  as the independent block, whereas the previously established unimodal PLS uses either  $X_{\text{PET}}$  or  $X_{\text{MRI}}$  for its respective PET or MRI analysis. For the informed PLS, which incorporated information about the subjects' group membership, the dependent block designated younger subjects as 1 and older subjects as 2. We note that our use of categorical variable in the informed multimodal PLS is inline with the classification of subjects into younger or older group. The agnostic PLS, on the other hand, is mainly oriented for extraction of covariance patterns and related latent variables rather than for classifications. In the following sections, we will refer to the independent block as  $X$  and the dependent block as  $Y$ .

### PLS with deflation

We adopted the PLS deflation scheme to deflate data matrices by discounting information projected onto the previous latent variable space, as described below. This computational

strategy guarantees the orthogonality of the extracted component in all data spaces (Hoegaerts et al., 2003).

The PLS uncovers the maximal covariance between a pair of latent variables, linearly constructed from each of the two respective datasets. Beginning with the original spatially standardized data matrices  $X$  and  $Y$ , the first latent variable pair is constructed as follows: The latent variable of  $X$  is  $t = \sum w_j x_j$  where  $w_j$  is a scalar for random variable  $x_j$  which is the  $j^{\text{th}}$  column of  $X$  ( $j=1, 2, \dots, P_X$ ). In matrix form,  $t=Xw$  where  $w=(w_1, w_2, \dots)^T$  with norm  $\|w\|=1$ . For the imaging dataset, index  $j$  refers to the  $j^{\text{th}}$  voxel in the brain volume. Similarly, the  $Y$  latent variable can be expressed as  $u=Yc$  ( $\|c\|=1$ ). Again, we refer to  $t$  and  $u$  as the first latent variable pair. In the context of the agnostic multimodal PLS, we refer to  $w$  and  $c$  as (the first) singular image of  $X$  and  $Y$ , respectively, as  $w$  and  $c$  can be mapped back to image space, displayed and interpreted. Assuming a zero mean, the covariance of the two latent variables,  $t$  and  $u$ , is therefore  $\text{cov}(t,u)=w'X'Yc$ . The maximal covariance value, with respect to  $w$  and  $c$ , can be proven to be the square root of the largest eigenvalue of the matrix  $\Omega=[X'YY'X]$  with  $w$  being the corresponding eigenvector of  $\Omega$ , and  $c$  being the corresponding eigenvector of  $Y'XX'Y$ . The second latent variable pair can be constructed in a similar way after the contributions of the first latent variable are regressed out (deflated) from  $X$  and  $Y$  as follows: Express

$$p_1 = \frac{X't}{\|t\|^2}, r_1 = \frac{Y'u}{\|u\|^2}$$

and calculate new  $X_1$  and  $Y_1$  as  $X_1 = X - tp_1'$ ,  $Y_1 = Y - tr_1'$ . The same procedure is then repeated for the new  $X_1$  and  $Y_1$  matrix pair to construct each subsequent latent variable pair, up to the  $L^{\text{th}}$  pair, where  $L=\text{rank}(X)$ . (The deflation scheme described here reflects the fact that  $Y$  is designated as the dependent datablock and  $X$  as the independent datablock.)

### Multi-block PLS

We use the term “dual-PLS” (DPLS) to refer to the previously described analysis of two complementary datasets, including one dependent datablock and one independent datablock. The DPLS is suitable for the agnostic multimodal PLS of the linkage between the patterns in two complementary imaging datasets (e.g.,  $X_{\text{PET}}$  and  $X_{\text{MRI}}$ ). In this case, DPLS is also suitable for the informed analysis of a single imaging data set since it is restricted to two complementary datasets. In order to analyze more than two complementary datasets (i.e., more than one independent block,  $X_1, X_2, \dots, X_m$ ), we introduce the “multi-block PLS”. The multi-block PLS is suitable for the agnostic analysis of three or more complementary imaging datasets, and it is suitable for the informed analysis of two or more datasets. Beginning with the original standardized data matrices  $X$  and  $Y$ , the multi-block PLS uncovers the first latent variable between  $Y$  and  $X=[X_1 X_2 \dots X_m]$  in exactly the same way as the DPLS. The previously described DPLS deflation step would mix contributions from different  $X$  blocks, making the results difficult to interpret. We implemented a previously suggested approach (Westerhuis and Smilde, 2001) for the multi-block PLS, deflating only the  $Y$ -block while keeping  $X$ -blocks untouched.

### Implementing the Agnostic Multimodal PLS by Reducing Matrix Size, a Computationally Efficient Method

The data matrix  $X_{\text{PET}}$  is  $n$  by  $P_X$  with  $n \ll P_X$  and consequently  $\text{rank}(X) \leq n$ . Without losing generality (as is usually the case with real data), we assume  $\text{rank}(X)=n$ . The matrix  $Y'X$  (or  $X'Y$ ) is prohibitively large for direct computation of its singular value (Bookstein, 1994) using the MATLAB built-in command `svds`.

To take advantage of the fact that  $n \ll P_X$  in the  $\Omega=X'YY'X$  related eigen-computation, we note that matrix  $YY'$  in the middle of  $X'YY'X$  is  $n$  by  $n$  and is a positive definite with full rank. Thus, there exists an  $n \times n$  positive definite (symmetric) matrix  $Z$  such that  $YY'=ZZ$ . Thus,  $\Omega=X'Z'ZX=(ZX)'ZX=A'A$ , where we have  $A=ZX$  which is  $n \times P_X$ . The eigenvalue computation of the

huge matrix  $A'A$  is equivalent to the eigenvalue computation of the much smaller matrix  $AA'$  which is  $n$  by  $n$ . In fact, let  $v_j$  be an eigenvector of  $A'A$  with eigenvalue  $\alpha$ :  $A'Av_j = \alpha v_j$ . Then,  $AA'Av_j = \alpha Av_j$ . In other words,  $w_j = Av_j$  is the eigenvector of the matrix  $AA'$  corresponding the same eigenvalue  $\alpha$ , and the inverse is, of course, also true. We numerically examined the computational stability of this approach by generating pairs of matrices,  $Y$  and  $X$ , of various sizes (but small enough to be handled by MATLAB. For this evaluation, the number of columns is greater than the number of rows of the generated matrices  $Y$  and  $X$ , and their ranks equal the number of rows. Both direct SVD of  $Y'X$  (the largest singular value) and the largest eigenvalue of  $Y'XX'Y$  were calculated. We found out that the two approaches produced numerically equivalent results.

Based on this mathematical reasoning, while the computation of the agnostic multimodal PLS may appear to be prohibitively expensive, it is actually quite manageable and requires no specialized or unusually high-performance computing hardware. (While the above procedure solves the PLS singular image  $w_j$  for data matrix  $X$ , the singular image  $c_j$  for data matrix  $Y$  can be simply obtained as  $c_j = Y't_j / \sqrt{\alpha}$  where  $t_j = Xw_j$ .) Moreover, this computationally efficient process can also be used for the non-parametric computation of linkage type-I errors, as described below.

### Agnostic Multimodal PLS versus Informed Multimodal PLS: Addressing Type I Errors

Three type-I errors, each with a unique nature, need to be considered in analyzing dual-imaging datasets via multimodal PLS. One of these three is related to agnostic multimodal PLS only and the other two to both agnostic and informed multimodal PLS.

**Linkage type-I error**—The agnostic multimodal PLS computes the linkage (as the maximal covariance) between patterns in these two complementary images blind to the subjects' information such as group membership or age. We define the *linkage type-I error* as the one for the squared correlation coefficient between the latent variable pair,  $t$  and  $u$ . The squared correlation coefficient characterizes the linkage between two complementary imaging datasets (We refer to it as the linkage index between the MRI and the PET datasets), and its type-I error is the probability of an observed/estimated linkage under the null hypothesis that there is no linkage between the two datasets (see our definition of non-linkage between two datasets in the Discussion section). Since  $t$  and  $u$  are constructed to maximize the covariance between them, the conventional parametric or non-parametric test cannot be used to assess the linkage type-I error. In the Discussion sections, we will propose a Monte-Carlo simulation procedure for assessing the linkage type-I error. Additional linkage type-I error assessment validation, however, will not be addressed in the current study. (We note that characterizing linkage type-I errors is only possible for the agnostic multimodal PLS, and not for the informed multimodal PLS.)

**Marker type-I error**—The multimodal PLS derived measurements, the numerical values of the latent variables, have the potential to be used to detect or track biologically or clinically relevant changes (e.g., distinguish different subject groups as demonstrated in this current study, characterize an individual's age or other state, and potentially tracking changes over time with additional validation we intend to conduct in future studies) with greater statistical power than conventional approaches. We characterize the type-I errors associated with the use of multimodal PLS-derived measurements as biological markers, which we call "*marker type-I errors*." In contrast to the agnostic multimodal PLS that permits us to estimate this type-I error conventionally as they are generated blind to the information for this subsequent usage, the informed multimodal PLS does not, since it identifies the linkage that most strongly distinguished, for example as in this current study, the two age groups. Thus, to assess informed multimodal PLS-derived marker type-I errors, non-parametric permutation strategies

(McIntosh et al., 2004; McIntosh and Lobaugh, 2004) will be used. To characterize the marker type-I error associated with the distinction between older and younger age groups for the informed multimodal PLS, 10,000 row-wise random permutations were performed on matrix Y and the multimodal PLS procedure was run for each of this permuted Y block and the unchanged X blocks. After performing the 10,000 permutations, we counted the number of permutations which misclassified a subject's age-group membership and used the histogram of unpaired t-test p-values over the 10,000 permutations to assess the marker type-I errors.

**Pattern type-I error**—This is the voxel-wise type-I errors in the singular images (the  $w$  and  $c$  singular images). It reflects the robustness of the regional/voxel-wise contribution to the inter-modality covarying patterns. With the data from all 29 subjects included in the agnostic multimodal PLS, the bootstrap resampling procedure proposed by a number of previous studies (McIntosh and Lobaugh, 2004) was run 100 times to estimate the voxel-wise standard deviation of the singular images. The Bootstrap estimated standard deviation was then used to scale the singular image pair for statistical significance assessment and visual inspection.

### **Characterizing the Agnostic multimodal PLS Power to Distinguish Subject Groups using Jackknife Method**

Although we are primarily interested in the marker type-I error assessment for the agnostic multimodal PLS, we also used a Jackknife procedure to examine the index/marker performance in terms of its power to classify the two age-groups. Agnostic multimodal PLS analysis was repeated 29 times, leaving one subject out each time. The resulting latent variable pair from the remaining 28 subjects was used to construct a linear discriminator which was then applied to determine the age-group membership of the excluded subject. This procedure allowed us to assess the classification accuracy of our PLS-derived measurements while considering potential cross-validation shrinkage for this sample.

### **Comparing the Agnostic multimodal PLS to SPM Analyses and Comparing Informed multimodal PLS to Unimodal Informed PLS**

We compared the agnostic and informed multimodal PLS approaches to established methods in terms of statistical power (i.e., statistical effect sizes in the discrimination between our older and younger subject groups) and type-I errors (i.e., the likelihood that the reported group difference is false). Effect sizes were characterized and compared using the conventional two-sample independent T-test or Hotelling  $T^2$  test. Since the correction for multiple comparisons for SPM analyses in calculating the effect is not feasible, the reported effect sizes for SPM analyses could be inflated, but still provide a measure by which to compare the different methods (or understate the superiority of the multimodal PLS method). Type-I errors for the informed multimodal PLS, which *simultaneously* generates latent variables for the subjects' PET and MRI images, the informed unimodal PLS analysis of their PET images, and the informed unimodal PLS analysis of the subjects' MRI gray matter images were characterized and compared using random permutation testing. We compared the Hotelling  $T^2$  test-based marker type-I errors associated with the agnostic multimodal PLS-derived latent variable pair, which is free of inflated effect sizes and free of multiple comparisons, --to those associated with the respective unimodal SPM analyses of the subjects' PET or MRI images (in the latter case using voxel-based morphometry) and with those using bi-modal SPM. To be consistent with the multimodal PLS analysis, the whole brain PET measurements and the total intracranial volume (TIV) were used to normalize the PET and MRI data respectively by proportional scaling together with the mask used in the multimodal PLS analysis. For the unimodal SPM analyses, coordinates with maximally significant differences were used to extract the data from each subject to characterize effect sizes for between-group differences, and compute the type-I errors with and without multiple comparison corrections. For the bi-modal SPM analyses,

PET and MRI measurements were treated as bi-variates at each voxel and to examine that dual-measurements are different between the two age groups.

We visually inspected and compared the spatial (parametric or covarying) patterns generated by each of the image-analysis algorithms. The spatial pattern is represented as a t-score map for each of the unimodal SPM analyses, as an F-score map for the bi-modal SPM analyses, as the simultaneously generated singular image pair for the agnostic multimodal PLS, as the simultaneously generated PET and MRI covariance patterns for the informed multimodal PLS, and as the independently generated covariance patterns for unimodal PET PLS and unimodal MRI PLS separately.

## RESULTS

Figure 1 shows each of the subjects' agnostic multimodal PLS-generated PET versus MRI latent variable subject scores (the numerical values of the variables  $t$  and  $u$ ), demonstrating no overlap between the older and younger subject groups. Figure 2 shows the distinction between older and younger subjects using the informed MRI PLS, informed PET PLS and informed PET-MRI multimodal PLS latent variable scores, demonstrating greatest separation between older and younger subjects using the informed multimodal PLS. Figure 3 shows the MRI and PET patterns generated using the agnostic multimodal PLS, the age-group-related MRI and PET patterns generating using informed multimodal PLS, unimodal MRI or PET PLS, and the conventional unimodal univariate MRI or PET SPM, and the age-group-related composite image generated using bi-modal PET-MRI SPM. This figure shows that the MRI and PET patterns simultaneously generated using multimodal PLS, with or without prior information about the subjects' age group, are similar to those MRI and PLS patterns independently generated from SPM or PLS analyses of either imaging modality alone. Finally for the agnostic multimodal PLS, we note that the overall linkage strength index, the squared correlation coefficient for the latent variable pair  $t$  and  $u$ , is  $R^2=0.73$  ( $p<3.77e-9$  and see Discussion Section for more on the marker type-I error).

*Agnostic multimodal PLS versus SPM in the discrimination between older and younger subject groups.* For unimodal univariate SPM PET, the maximally significant group difference (one-tailed, in right fronto-temporal cortex) was  $p=2e-7$  and 0.004, before and after correction for multiple comparisons, and the corresponding effect size was 2.43. For unimodal univariate SPM MRI (i.e., gray matter VBM), the maximally significant group difference (one-tailed, in right parietal cortex) was  $p=1e-11$  and  $1e-5$ , before and after multiple comparisons, and the effect size was 4.11). For bi-modal SPM, the maximally significant group difference (in right frontal cortex) was  $p=1e-12$  and  $1e-7$ , before and after multiple comparisons and the effect size was 5.01. By comparison, for agnostic multimodal PLS, the significant group difference was  $p=4e-13$  and the effect size was 5.21 *without the need* to correct multiple comparisons. Note the effect sizes associated with all three SPM analyses were performed without adjustment for multiple comparisons and are thus likely to be inflated. As shown in figure 1, when we plot the respective PET and MRI latent variable scores for the younger and older subjects, there was no overlap between groups.

In addition to assessing the statistical inference type-I error, we used Jackknife analysis to evaluate its ability to classify subjects into older and younger age groups. For each iteration, data from one subject was left out, a linear classifier was computed, and we calculated the accuracy of the classifier to predict the remaining subject's age group. Using this approach, the agnostic multimodal PLS procedure permitted us to accurately classify the left out subject's age group 100% of the time.

*Informed PLS using PET only, MRI only, or PET and MRI together in the discrimination between older and younger subject groups.* Out of 10,000 random permutations in which subject age group-membership was exchanged, we computed the number of permutations associated with a distinction in group membership as strong as the original comparison, providing information about type-I errors. Using this approach, the type-I error rate was 30 ( $p=0.003$ ) for unimodal PET PLS, 2 ( $p=0.0002$ ) for unimodal MRI PLS and 0 ( $p=0.0000$ ) using PET-MRI multimodal PLS. Effect sizes for the discrimination between older and younger subjects was 3.25 using informed PET PLS, 4.27 using informed MRI PLS, and 4.85 using informed PET-MRI PLS.

As shown in figure 3, the MRI and PET patterns simultaneously generated using either the agnostic or informed multimodal PLS were quite similar to those generated in independent analyses of either the subjects' MRI or PET images using the conventional PLS and SPM methods, *providing support for the use of our new multimodal image-analysis technique.* For example, agnostic multimodal PLS simultaneously generated the PET and MRI covariance patterns (i.e., singular images) shown in the top row of figure 3. These images were created with a threshold of  $p=0.05$  for both positive and negative values using bootstrap-generated standard errors and 100 iterations. The covarying pattern revealed significantly lower medial and superior frontal, anterior and middle cingulate measurements (negative pattern weights) in both the MRI and PET singular maps, consistent with the pattern in the other maps and findings from previous MRI, PET, and neuropathological studies suggesting that normal aging preferentially affects frontal regions. In addition, the covarying pattern revealed significantly lower inferior frontal and posterior cingulate measurements only in the PET singular image--indeed, with increased measurements, reflecting relative sparing in inferior frontal cortex, again consistent with the pattern found in the other maps.

### Computational Speed

For both the agnostic multimodal PLS and informed multimodal PLS, the computational speed is compatible to the statistical part of a routine SPM analysis.

## DISCUSSION

In this study, we proposed the use of multimodal PLS to characterize the covarying patterns among two or more complementary complex data sets. The technique could be used to characterize the linkage between the patterns of functional and structural brain images in a group analysis, or as previously suggested, between a person's EEG data and fMRI time series (Martinez-Montes et al., 2004). Further, it could be used to combine, and capitalize on, information from complementary data sets independent of any additional information (i.e., agnostically) or in relationship to known information (e.g., "informed" about a person's age, genetic background, or clinical, biological, or neuropsychological state). PLS is one of several tools which can be potentially used for studying the inter-modality multi-imaging datasets. Not only can it be used to analyze multiple data sets in an exploratory fashion to generate information for subsequent model-based analyses and hypothesis testing (see (Rajah and McIntosh, 2005) as in intra-modality PLS), but more importantly, it can construct a latent variable-based index/marker that could subsequently be used to characterize group differences (e.g., AD patients versus controls), longitudinal changes (e.g., the progression of AD-associated brain changes), and effects of putative treatments (e.g., putative AD-slowing, risk-reducing or prevention therapies).

As a proof-of-principle, we illustrated the promise of the multimodal PLS by the improvement of our ability to distinguish between 15 younger and 14 older subjects (applying it with or without the subjects' age information). Since the current findings may be driven partly by the distinct subject groups, additional studies will be needed to determine the extent to which it

improves power to characterize more subtle effects. In a preliminary study, we found that multimodal PLS provided better power than FDG-PET or MRI alone in discriminating carriers from non-carriers of apolipoprotein E (APOE)  $\epsilon 4$  gene, the major genetic risk factor for Alzheimer's disease (unpublished data). *Additional studies are needed to compare the multimodal PLS with other multi-modal multivariate image-analysis techniques, such as Fisher discriminant analysis and support vector machine. Additional studies are also needed to determine the extent to which the multimodal PLS could be improved by incorporating other procedures, such as penalized logistic regression (Fort and Lambert-Lacroix, 2005) and smoothness constraints (Kustra and Strother, 2001).*

The observed different performances by the agnostic multivariate multimodal PLS and the general linear model-based massive univariate SPM can be partially explained by the different theories of these two approaches. For multimodal PLS, pieces of information from all voxels over the whole brain volume are combined and differential contribution of each voxel is reflected by its weight. Instead of combining all voxels to generate an integrated index, the massive univariate SPM approach with correction of family-wise error selects only few of the most significant ones among all voxels. This selection process could be thought of as an extreme case of combination of voxels with weight 1 for the most significant voxel and weight 0 for all others. Instead of performing complementary multivariate or univariate analyses separately, additional future studies are needed to examine the possibility of combining these two techniques to further improve sensitivity.

As indicated in the method section, while the dual-block PLS is a special case, it is also the foundation for the general multi-block PLS which can handle data from more than two complementary data sets. In this study, we used the multi-block PLS for informed multimodal PLS to find the linkage between FDG PET and volumetric MRI patterns that best distinguished subjects in older and younger subject groups, such that age group membership was an additional (and only dependent) data set. Considering the successful application of multi-block PLS analysis in the field of chemometrics (Lopes et al., 2002; Westerhuis et al., 1996; Westerhuis et al., 1997; Westerhuis and Smilde, 2001), we are interested in extending the multi-block PLS to other brain imaging and non-imaging data sets. For instance, we are interested in characterizing the linkage among three complementary data sets (e.g., FDG PET, fibrillar amyloid images, and volumetric MRI) in either the agnostic or informed mode (i.e., with or without the use of additional dependent information, such as a person's clinical classification).

In this study, the comparison between younger and older subjects was used to provide face validity for our proposed multimodal PLS and demonstrate both its potential advantages and comparability to conventional unimodal image-analysis techniques. Thus, we demonstrated the superiority of the multimodal PLS to discriminate between older and younger subject groups, free from multiple comparisons, and simultaneously generated covariance patterns in the subjects' MRI and PET images which resembled those generated interdentally in the MRI or PET images using either unimodal SPM and unimodal PLS. In doing so, it found lower CMRgl and gray matter covariance patterns in frontal regions. Like previous FDG PET, volumetric MRI, and neuropathological studies measuring reductions in synaptic density (Alexander et al., 2006; Good et al., 2001; Hof and Morrison, 2004; Kuhl et al., 1982; Loessner et al., 1995; Moeller et al., 1996; Reiman et al., 1996; Reiman et al., 2004; Salmon et al., 1991; Terry et al., 2004; Alexander et al., 2008), our studies suggest that normal aging preferentially affects these and other brain regions. While this example illustrates the potential to relate covariance patterns to biological features of the condition being studied, additional research is needed to determine the biological significance of multimodal PLS-derived subject scores and the covariance patterns to which they are related to.

We introduced the squared correlation coefficient of the latent variable pair as one linkage index between two image modalities for agnostic multimodal PLS. Another one, an image-wise index, provides information about explanatory power of the independent X datablock as a whole for each voxel location in the dependent Y datablock. This index consists of a correlation coefficient map over Y. For each voxel in Y, the correlation coefficient is the one between the single latent variable of the X-block and the measurement from this voxel. In our agnostic PLS where MRI was treated as an X-block, the overall explanatory power is the overall anatomical influence on the FDG-PET spatial pattern. The explanatory power maps can be interpreted easily as correlation maps. We calculated this image-wise index and found it was very similar to the singular image in Figure 3. The image-wise index provides localized effects on one image modality by the overall influence of another (however, we caution the interpretation of this relationship as causality). With further validation, the alternation of the localized effects can possibly be used as a marker for disease diagnosis and monitoring of disease progressions.

We demonstrated the superior performance of multimodal PLS in distinguishing the two age groups. The multimodal PLS not only extracted the covarying patterns within each image modality but also integrated them across modalities. Since it is voxel-based, the multimodal PLS method ensures the richness of information in the neuroimaging data is utilized to its fullest extent. Moreover, the multivariate approach (the use of the summarized index) is free of multiple comparisons. Therefore, it may be possible to characterize the longitudinal changes in multimodal PLS-derived subject scores (and the covariance patterns to which they are related), and subsequently test the efficacy of putative AD-slowing treatments to modify these particular scores and covariance patterns without the need to correct for multiple comparisons.

In addition to introducing the multimodal PLS, we have suggested how it can be performed with rigorous statistical type-I error evaluations. We distinguished three different type-I errors, placing particular emphasis on *marker type-I errors*, and suggested how multimodal PLS-derived subject scores could capitalize on all of the information in a subject's images. A conventional parametric strategy was used to estimate the marker type-I errors for the agnostic multimodal PLS, and the previously proposed permutation method (McIntosh et al., 2004; McIntosh and Lobaugh, 2004) was used to do so for the informed multimodal PLS. For both agnostic multimodal PLS and informed multimodal PLS, *pattern type-I error* can be evaluated using the bootstrap resampling technique (McIntosh et al., 2004). A potential alternative to this computationally expensive approach is the random matrix theory based statistical inference method (Johnstone, 2001) which we will investigate in future studies. The *linkage type-I error*, is unique to the agnostic multimodal PLS and was not fully investigated in the current study. As mentioned earlier, the conventional parametric assessment of the linkage type-I error is problematic since the agnostic multimodal PLS seeks to maximize covariance between the latent variable pair. Nevertheless, we suggested the use of the Monte-Carlo simulation as a way to assess this type-I errors. In performing the Monte-Carlo simulation, we assume that the two imaging datasets are uncorrelated (any variable in dataset X has zero correlation with any variable in dataset Y). The Monte-Carlo simulation could also be used to assess the type-I errors associated with any null hypothesis such as the mean/median/minimum correlation coefficient among cross dataset variable pairs is with a given value, or the correlation coefficient is with a specific statistical distribution. Although the Monte-Carlo simulation procedure is computationally complex, it is feasible to use in conjunction with our computationally efficient algorithm, which can be used whenever the number of subjects and scans is much smaller than the number of voxels. Furthermore, it is theoretically possible that the dimensions used in the Monte-Carlo simulation can be reduced even further. While we have outlined the linkage type-I error issues here, we believe that this interesting and challenging topic merits further study.

The multimodal PLS can be performed either informed to the variable of interest or agnostic to this additional information. Investigators may want to pre-specify which of these two methods to use in the data analysis. The informed PLS will find the linkage pattern most strongly associated with the variable of interest; but it requires additional computations for non-parametric test (e.g., permutation) or Monte Carlo simulation to properly estimate Type I error. The informed PLS may not be associated with significantly better discrimination power than the agnostic PLS when, for example, the contribution of the variable of interest to the linkage pattern far outweighs the contributions of other variables.

In conclusion, we introduce a new voxel-based multivariate image analysis technique to simultaneously characterize covarying patterns in complementary brain images from the same person. It capitalizes on all of the information available from these complementary data-sets. In our very first application of this method, we found that it distinguished between older and younger subjects with better power than unimodal SPM and PLS analyses of the subjects' PET or MRI images alone, and with no need to correct for multiple comparisons. While the superior performance of multimodal PLS method was demonstrated in the current study using data pre-processed by the SPM2 software package, we expect multimodal PLS to be useful using other versions of SPM and potentially with other image processing platforms. Further, we believe this technique has the potential to link patterns of information among any number of complementary images from an individual, use other kinds of complementary complex datasets besides brain images, and characterize individual state- or trait-dependent brain patterns in a more powerful way.

## Acknowledgments

Earlier versions of this work were presented at the World Congress on Medical Physics and Biomedical Engineering, Aug, 2003, Australia, the Nuclear Medicine Annual meeting, June, 2004, and the 9th International Conference on Alzheimer's Disease and Related Disorders, 2004. This work was supported by the NIMH (MH57899), NIA (P30AG19610, AG025526, MH57899), the Alzheimer's Association (IIRG-98-068, IIRG-98-078, and IIRG-02-3784), the Mayo Clinic and Banner Alzheimer's Foundations, and the Arizona Department of Health Services. The authors thank Wendy Lee, Sandy Goodwin, Les Mullen, Pat Raso, Debbie Intorcchia, Anita Prouty, Cole Reschke, Xiaofen Liu, Justin Venditti, Dr. Lawrence Mayer and Dr. Richard Gerkin for their support.

## References

- Alexander GE, Chen K, Aschenbrenner M, Merkle TL, Santerre-Lemmon L, Shamy JL, Skaggs WE, Buonocore MH, Rapp PR, Barnes CA. Age-related regional network of magnetic resonance imaging gray matter in the rhesus macaque. *J Neurosci* 2008;28:2710–2718. [PubMed: 18337400]
- Alexander GE, Chen K, Merkle TL, Reiman EM, Caselli RJ, Aschenbrenner M, Santerre-Lemmon L, Lewis DJ, Pietrini P, Teipel SJ, Hampel H, Rapoport SI, Moeller JR. Regional network of magnetic resonance imaging gray matter volume in healthy aging. *Neuroreport* 2006;17:951–956. [PubMed: 16791083]
- Alexander GE, Mentis MJ, Van Horn JD, Grady CL, Berman KF, Furey ML, Pietrini P, Rapoport SI, Schapiro MB, Moeller JR. Individual differences in PET activation of object perception and attention systems predict face matching accuracy. *Neuroreport* 1999;10:1965–1971. [PubMed: 10501542]
- Alexander GE, Moeller JR. Application of the Scaled Subprofile model, a statistical approach to the analysis of functional patterns in neuropsychiatric disorders, A principal component approach to modeling regional patterns of brain function in disease. *Human Brain Mapping* 1994:79–94.
- Anderson ND, Iidaka T, Cabeza R, Kapur S, McIntosh AR, Craik FI. The effects of divided attention on encoding- and retrieval-related brain activity: A PET study of younger and older adults. *J Cogn Neurosci* 2000;12:775–792. [PubMed: 11054920]
- Ashburner J, Friston K. Multimodal image coregistration and partitioning--a unified framework. *Neuroimage* 1997;6:209–217. [PubMed: 9344825]
- Bookstein FL. Partial least squares, A dose-response model for measurement in the behavioral and brain sciences. *Psychology [an electronic journal]* 1994;5(23)

- Calhoun VD, Adali T, Pearlson GD, Pekar JJ. Spatial and temporal independent component analysis of functional MRI data containing a pair of task-related waveforms. *Hum Brain Mapp* 2001;13:43–53. [PubMed: 11284046]
- Calhoun VD, Adali T, Pekar JJ, Pearlson GD. Latency (in)sensitive ICA. Group independent component analysis of fMRI data in the temporal frequency domain. *Neuroimage* 2003;20:1661–1669. [PubMed: 14642476]
- Casanova R, Srikanth R, Baer A, Laurienti PJ, Burdette JH, Hayasaka S, Flowers L, Wood F, Maldjian JA. Biological parametric mapping, A statistical toolbox for multimodality brain image analysis. *Neuroimage* 2007;34:137–143. [PubMed: 17070709]
- Chen H, Yao D, Zhou K, Zhou T, Zhuo Y, Chen L. A method based on independent component analysis for processing fMRI data. *Sheng Wu Yi Xue Gong Cheng Xue Za Zhi* 2002;19:64–66. [PubMed: 11951526]
- Espósito F, Seifritz E, Formisano E, Morrone R, Scarabino T, Tedeschi G, Cirillo S, Goebel R, Di SF. Real-time independent component analysis of fMRI time-series. *Neuroimage* 2003;20:2209–2224. [PubMed: 14683723]
- Feigin A, Leenders KL, Moeller JR, Missimer J, Kuenig G, Spetsieris P, Antonini A, Eidelberg D. Metabolic network abnormalities in early Huntington's disease, an [(18)F]FDG PET study. *J Nucl Med* 2001;42:1591–1595. [PubMed: 11696626]
- Fort G, Lambert-Lacroix S. Classification using partial least squares with penalized logistic regression. *Bioinformatics* 2005;21:1104–1111. [PubMed: 15531609]
- Friston KJ. Functional and effective connectivity, A synthesis. *Human Brain Mapping* 1994;56–78.
- Friston KJ, Harrison L, Penny W. Dynamic causal modelling. *Neuroimage* 2003;19:1273–1302. [PubMed: 12948688]
- Good CD, Johnsrude IS, Ashburner J, Henson RN, Friston KJ, Frackowiak RS. A voxel-based morphometric study of ageing in 465 normal adult human brains. *Neuroimage* 2001;14:21–36. [PubMed: 11525331]
- Grady C, McIntosh A, Rajah M, Craik F. Neural correlates of the episodic encoding of pictures and words. *Proc Natl Acad Sci U S A* 1998;95:2703–2708. [PubMed: 9482951]
- Habeck C, Krakauer J, Ghez C, Sackeim H, Eidelberg D, Stern Y, Moeller JR. A new approach to spatial covariance modeling of functional brain imaging data, ordinal trend analysis. *Neural Comput* 2005;17:1602–1645. [PubMed: 15901409]
- Habib R, McIntosh AR, Wheeler MA, Tulving E. Memory encoding and hippocampally-based novelty/familiarity discrimination networks. *Neuropsychologia* 2003;41:271–279. [PubMed: 12457753]
- Hoegaerts, L.; Suykens, JAK.; Vandewalle, J.; De Moor, B. Kernel PLS variants for regression. *Proc. of the 11th European Symposium on Artificial Neural Networks*; 2003. p. 203-208.
- Hof PR, Morrison JH. The aging brain, morphomolecular senescence of cortical circuits. *Trends Neurosci* 2004;27:607–613. [PubMed: 15374672]
- Ibanez V, Pietrini P, Alexander GE, Furey ML, Teichberg D, Rajapakse JC, Rapoport SI, Schapiro MB, Horwitz B. Regional glucose metabolic abnormalities are not the result of atrophy in Alzheimer's disease. *Neurology* 1998;50:1585–1593. [PubMed: 9633698]
- Iidaka T, Anderson ND, Kapur S, Cabeza R, Craik FI. The effect of divided attention on encoding and retrieval in episodic memory revealed by positron emission tomography. *J Cogn Neurosci* 2000;12:267–280. [PubMed: 10771411]
- Jack CR Jr, Lowe VJ, Senjem ML, Weigand SD, Kemp BJ, Shiung MM, Knopman DS, Boeve BF, Klunk WE, Mathis CA, Petersen RC. 11C PiB and structural MRI provide complementary information in imaging of Alzheimer's disease and amnesic mild cognitive impairment. *Brain* 2008;131:665–680. [PubMed: 18263627]
- Keightley ML, Winocur G, Graham SJ, Mayberg HS, Hevenor SJ, Grady CL. An fMRI study investigating cognitive modulation of brain regions associated with emotional processing of visual stimuli. *Neuropsychologia* 2003;41:585–596. [PubMed: 12559151]
- Kuhl DE, Metter EJ, Riege WH, Phelps ME. Effects of human aging on patterns of local cerebral glucose utilization determined by the [18F]fluorodeoxyglucose method. *J Cereb Blood Flow Metab* 1982;2:163–171. [PubMed: 6978885]

- Kustra R, Strother S. Penalized discriminant analysis of [15O]-water PET brain images with prediction error selection of smoothness and regularization hyperparameters. *IEEE Trans Med Imaging* 2001;20:376–387. [PubMed: 11403197]
- Loessner A, Alavi A, Lewandrowski KU, Mozley D, Souder E, Gur RE. Regional cerebral function determined by FDG-PET in healthy volunteers, normal patterns and changes with age. *J Nucl Med* 1995;36:1141–1149. [PubMed: 7790936]
- Lopes JA, Menezes JC, Westerhuis JA, Smilde AK. Multiblock PLS analysis of an industrial pharmaceutical process. *Biotechnol Bioeng* 2002;80:419–427. [PubMed: 12325150]
- Martinez-Montes E, Valdes-Sosa PA, Miwakeichi F, Goldman RI, Cohen MS. Concurrent EEG/fMRI analysis by multiway Partial Least Squares. *Neuroimage* 2004;22:1023–1034. [PubMed: 15219575]
- McIntosh AR. Mapping cognition to the brain through neural interactions. *Memory* 1999;7:523–548. [PubMed: 10659085]
- McIntosh AR. Understanding neural interactions in learning and memory using functional neuroimaging. *Ann N Y Acad Sci* 1998;855:556–571. [PubMed: 9929651]
- McIntosh AR, Bookstein FL, Haxby JV, Grady CL. Spatial pattern analysis of functional brain images using partial least squares. *Neuroimage* 1996;3:143–157. [PubMed: 9345485]
- McIntosh AR, Chau WK, Protzner AB. Spatiotemporal analysis of event-related fMRI data using partial least squares. *Neuroimage* 2004;23:764–775. [PubMed: 15488426]
- McIntosh AR, Gonzalez-Lima F. Structural equation modeling and its application to network analysis in functional brain imaging. *Human Brain Mapping* 1994;2–22.
- McIntosh AR, Lobaugh NJ. Partial least squares analysis of neuroimaging data, applications and advances. *Neuroimage* 2004;23(Suppl 1):S250–S263. [PubMed: 15501095]
- McKeown MJ, Sejnowski TJ. Independent component analysis of fMRI data, examining the assumptions. *Hum Brain Mapp* 1998;6:368–372. [PubMed: 9788074]
- Moeller JR, Ishikawa T, Dhawan V, Spetsieris P, Mandel F, Alexander GE, Grady C, Pietrini P, Eidelberg D. The metabolic topography of normal aging. *J Cereb Blood Flow Metab* 1996;16:385–398. [PubMed: 8621743]
- Moeller JR, Strother SC, Sidtis JJ, Rottenberg DA. Scaled subprofile model, a statistical approach to the analysis of functional patterns in positron emission tomographic data. *J Cereb Blood Flow Metab* 1987;7:649–658. [PubMed: 3498733]
- Moritz CH, Houghton VM, Cordes D, Quigley M, Meyerand ME. Whole-brain functional MR imaging activation from a finger-tapping task examined with independent component analysis. *AJNR Am J Neuroradiol* 2000;21:1629–1635. [PubMed: 11039341]
- Nestor PG, O'Donnell BF, McCarley RW, Niznikiewicz M, Barnard J, Jen SZ, Bookstein FL, Shenton ME. A new statistical method for testing hypotheses of neuropsychological/MRI relationships in schizophrenia, partial least squares analysis. *Schizophr Res* 2002;53:57–66. [PubMed: 11728838]
- O'Donnell BF, McCarley RW, Potts GF, Salisbury DF, Nestor PG, Hirayasu Y, Niznikiewicz MA, Barnard J, Shen ZJ, Weinstein DM, Bookstein FL, Shenton ME. Identification of neural circuits underlying P300 abnormalities in schizophrenia. *Psychophysiology* 1999;36:388–398. [PubMed: 10352563]
- Rajah MN, McIntosh AR. Overlap in the functional neural systems involved in semantic and episodic memory retrieval. *J Cogn Neurosci* 2005;17:470–482. [PubMed: 15814006]
- Rajah MN, McIntosh AR, Grady CL. Frontotemporal interactions in face encoding and recognition. *Brain Res Cogn Brain Res* 1999;8:259–269. [PubMed: 10556604]
- Reiman EM, Caselli RJ, Yun LS, Chen K, Bandy D, Minoshima S, Thibodeau SN, Osborne D. Preclinical evidence of Alzheimer's disease in persons homozygous for the epsilon 4 allele for apolipoprotein E. *N Engl J Med* 1996;334:752–758. [PubMed: 8592548]
- Reiman EM, Chen K, Alexander GE, Caselli RJ, Bandy D, Osborne D, Saunders AM, Hardy J. Functional brain abnormalities in young adults at genetic risk for late-onset Alzheimer's dementia. *Proc Natl Acad Sci U S A* 2004;101:284–289. [PubMed: 14688411]
- Salmon E, Maquet P, Sadzot B, Degueldre C, Lemaire C, Franck G. Decrease of frontal metabolism demonstrated by positron emission tomography in a population of healthy elderly volunteers. *Acta Neurol Belg* 1991;91:288–295. [PubMed: 1781265]

- Schmithorst VJ, Holland SK. Comparison of three methods for generating group statistical inferences from independent component analysis of functional magnetic resonance imaging data. *J Magn Reson Imaging* 2004;19:365–368. [PubMed: 14994306]
- Smith JF, Chen K, Johnson S, Morrone-Strupinsky J, Reiman EM, Nelson A, Moeller JR, Alexander GE. Network analysis of single-subject fMRI during a finger opposition task. *Neuroimage* 2006;32:325–332. [PubMed: 16733091]
- Terry RD, DeTeresa R, Hansen LA. Neocortical cell counts in normal human adult aging. *Ann Neurol* 2004;21:530–539. [PubMed: 3606042]
- Westerhuis JA, Coenegracht PMJ, Lerk CF. Multivariate modelling of the tablet manufacturing process with wet granulation for tablet optimization and in-process control. *Int J Pharmaceut* 1997;156:109–117.
- Westerhuis JA, de Haan P, Zwinkels J, Jansen WT, Coenegracht PMJ, Lerk CF. Optimisation of the composition and production of mannitol/microcrystalline cellulose tablets. *Int J Pharmaceut* 1996;143:151–162.
- Westerhuis JA, Smilde AK. Deflation in multiblock PLS. *Journal of Chemometrics* 2001;15:485–493.
- Worsley KJ, Poline JB, Friston KJ, Evans AC. Characterizing the response of PET and fMRI data using multivariate linear models. *Neuroimage* 1997;6:305–319. [PubMed: 9417973]

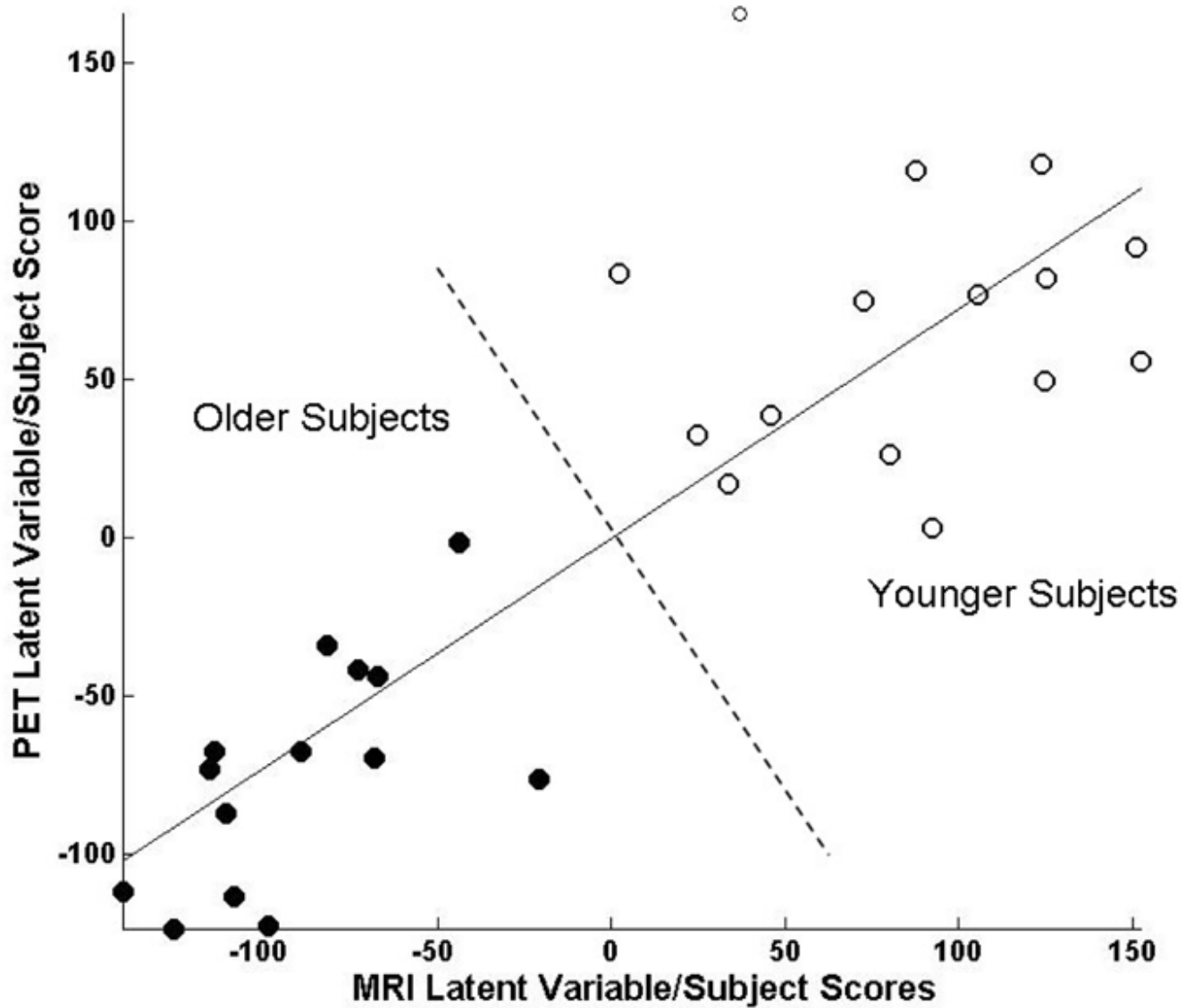


**Figure 1.** Scatter graph of MRI-PET subject (i.e., latent variable pair) scores generated using the agnostic multimodal PLS, corresponding to  $t$ , the MRI latent variable on the x-axis and  $u$ , the PET latent variable, on the y-axis). Solid circles denote subjects in the older age group and open circles denote those in the younger age group. Note the complete separation (indicated by the dashed line) between the older and younger subjects. The solid line is the latent variable line of regression between MRI and PET subject scores.

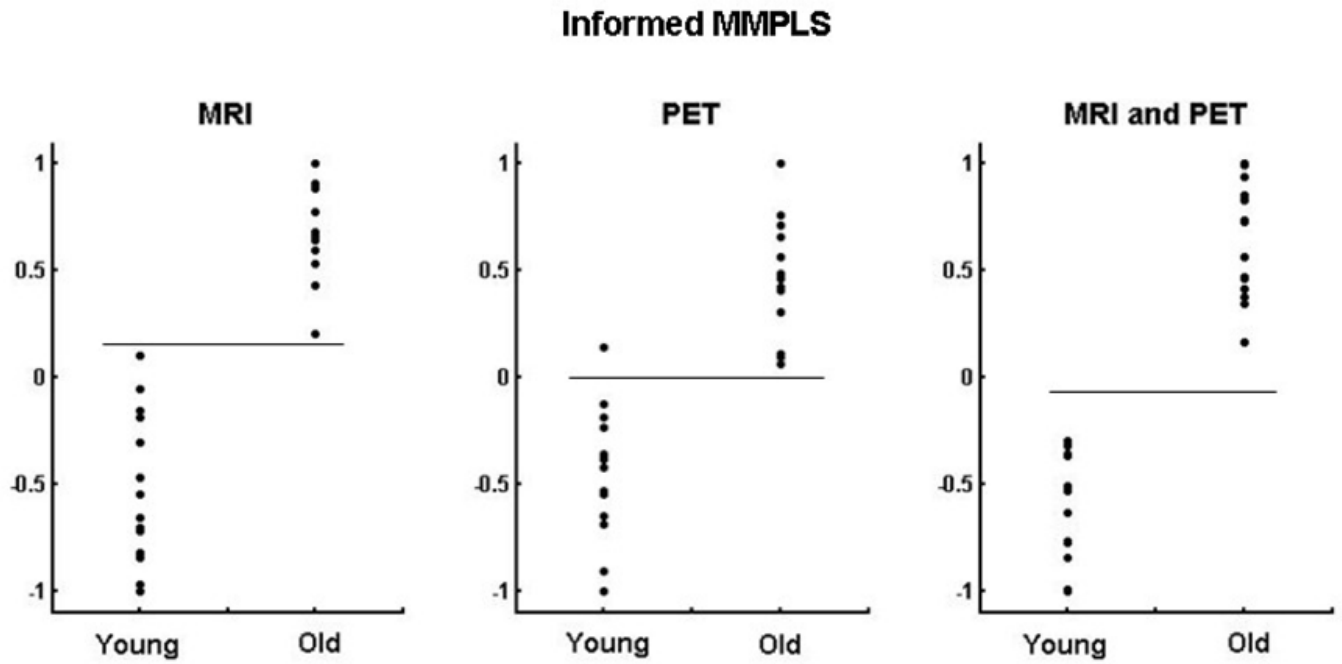


**Figure 2.** Scatter graph of subject scores generated using the informed unimodal PET PLS (left panel), the informed unimodal MRI PLS (central panel), and the informed multimodal PLS (right panel). Note the greater separation between the multimodal PLS-generated older and younger subject scores.

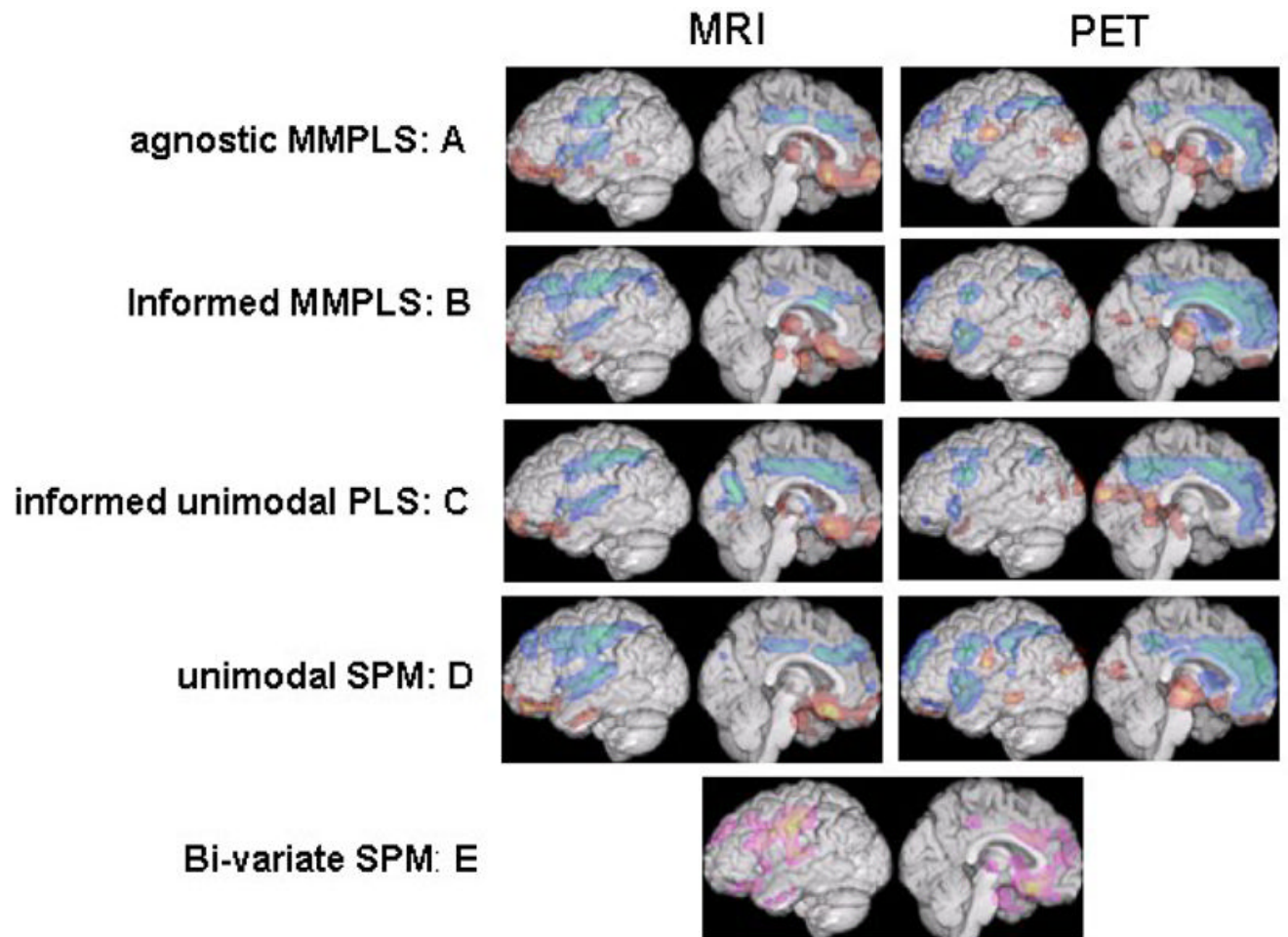


**Figure 3.**

MRI and PET spatial patterns simultaneously characterized using the agnostic multimodal PLS (Panel A) and informed multimodal PLS (Panel B), the MRI and PET spatial patterns independently characterized using the unimodal PLS (Panel C) and SPM (Panel D) and the combined MRI and PET pattern generated using bi-variate SPM (Panel E)